Neuro-Oncology
26(4), 640–652, 2024 | https://doi.org/10.1093/neuonc/noad231 | Advance Access date 23 December 2023

Whole tumor analysis reveals early origin of the *TERT* promoter mutation and intercellular heterogeneity in *TERT* expression

Christina L. Appin, Chibo Hong, Abigail K. Suwala, Stephanie Hilz, Radhika Mathur, David A. Solomon, Ivan V. Smirnov, Nicholas O. Stevers, Anny Shai, Albert Wang, Mitchel S. Berger, Susan M. Chang, Joanna J. Phillips, and Joseph F. Costello

All author affiliations are listed at the end of the article

Corresponding Author: Joseph Costello, PhD, Department of Neurological Surgery, University of California San Francisco, 1450 3rd Street, San Francisco, CA 94158, USA. (Joseph.costello@ucsf.edu).

Abstract

Background. The *TERT* promoter mutation (TPM) is acquired in most *IDH*-wildtype glioblastomas (GBM) and *IDH*-mutant oligodendrogliomas (OD) enabling tumor cell immortality. Previous studies on TPM clonality show conflicting results. This study was performed to determine whether TPM is clonal on a tumor-wide scale.

Methods. We investigated TPM clonality in relation to presumed early events in 19 *IDH*-wildtype GBM and 10 *IDH*-mutant OD using 3-dimensional comprehensive tumor sampling. We performed Sanger sequencing on 264 tumor samples and deep amplicon sequencing on 187 tumor samples. We obtained tumor purity and copy number estimates from whole exome sequencing. *TERT* expression was assessed by RNA-seq and RNAscope.

Results. We detected TPM in 100% of tumor samples with quantifiable tumor purity (219 samples). Variant allele frequencies (VAF) of TPM correlate positively with chromosome 10 loss in GBM ($R = 0.85$), *IDH1* mutation in OD ($R = 0.87$), and with tumor purity ($R = 0.91$ for GBM; $R = 0.90$ for OD). In comparison, oncogene amplification was tumor-wide for *MDM4*- and most *EGFR*-amplified cases but heterogeneous for *MYCN* and *PDGFRA*, and strikingly high in low-purity samples. TPM VAF was moderately correlated with *TERT* expression ($R = 0.52$ for GBM; $R = 0.65$ for OD). *TERT* expression was detected in a subset of cells, solely in TPM-positive samples, including samples equivocal for tumor.

Conclusions. On a tumor-wide scale, TPM is among the earliest events in glioma evolution. Intercellular heterogeneity of *TERT* expression, however, suggests dynamic regulation during tumor growth. *TERT* expression may be a tumor cell-specific biomarker.

Key Points

- The *TERT* promoter mutation occurs very early in tumor evolution.
- *TERT* expression is heterogeneous within individual tumor samples.
- *TERT* expression is a potential tumor cell-specific marker that could be useful in cases equivocal for tumor.

Telomeres are composed of 6 base pair repeats which are added by telomerase to the ends of eukaryotic chromosomes.[1–3] Telomere-specific proteins of the shelterin complex bind and cap the telomeres, thereby protecting them from degradation and fusion events.[4,5] As telomerase is absent in somatic cells, their telomeres shorten with each successive cell division, eventually leading to cell senescence or death.[1–3] To bypass senescence and attain replicative immortality, cells re-activate telomerase or acquire the alternative lengthening of telomeres phenotype via loss of function of ATRX or SMARCAL.[6–9] The *TERT* promoter mutation (TPM), a single nucleotide substitution typically in 1 of 2 positions (G228A or G250A), reactivates *TERT* transcription and telomerase activity.[10] Infiltrating gliomas commonly harboring *TERT* promoter mutations include *IDH*-wildtype GBM and *IDH*-mutant OD.[11]

© The Author(s) 2023. Published by Oxford University Press on behalf of the Society for Neuro-Oncology. All rights reserved.
For permissions, please e-mail: journals.permissions@oup.com

Importance of the Study

TERT promoter mutation (TPM) is present in most *IDH*-wildtype glioblastomas (GBM) and *IDH*-mutant oligodendrogliomas (OD), among other tumor types, reactivating telomerase and enabling limitless cell division that defines the immortal state. TPM-mediated reactivation of telomerase is tumor-specific, suggesting strategies for tumor-selective reversal of immortality. Most previous studies used limited tumor sampling to examine clonality of TPM and other mutations leading to conflicting conclusions and potentially inaccurate evolutionary models. Pinpointing the evolutionary timing of TPM is critical to understanding its role in tumorigenesis, for building accurate tumor models, and for assessing the value of therapeutic targeting. Here we used a 3D maximal tumor sampling approach along with deep sequencing to address these important issues.

Tumor cell immortality via the TPM is potentially reversible and therefore remains a promising area to explore new therapeutic targets. The transcription factor GABP binds and activates the mutant *TERT* promoter, as well as rare but recurrent 21–25 base pair duplications,[12] but does not bind the wildtype *TERT* promoter.[13] Targeting GABP or upstream regulators,[14–17] therefore, offers the potential for selective elimination of TPM-positive cancer cells.

Intratumor heterogeneity contributes to treatment failures,[18–20] as subclones lacking a therapeutic target will survive therapy and may rapidly repopulate the tumor during treatment.[21–24] The ideal therapeutic target, therefore, would be a mutation that arises in the earliest stages of tumor evolution and persists in all regions of the tumor and in all tumor cells. Several studies have reported on TPM clonality and evolutionary timing in glioma,[25–29] however, the conclusions are mostly based on limited tumor sampling and most do not quantify tumor purity which is a confounding factor. Sequencing depth also varies across studies. We have designed a study using whole-tumor sampling and deep sequencing to investigate the spatial distribution of TPM in *IDH*-wildtype GBM and *IDH*-mutant OD. We collected up to 10 samples per tumor to maximally represent the whole tumor and estimated the tumor purity of each from exome sequencing. Registering the 3D spatial coordinates of each sample to the MRI-defined tumor confirmed maximal tumor sampling. We performed deep amplicon sequencing to provide adequate sequencing depth, particularly in samples with lower purity, in addition to Sanger sequencing which was performed on all samples. This design allowed us to go beyond the limitations of single-sample analysis and low-depth sequencing to rigorously examine clonality of TPM on a tumor-wide scale. Our study provides insight into the relationship between TPM and tumor purity in the context of other presumed early genetic alterations and characteristic oncogene amplifications and reveals an unexpected relationship with *TERT* expression.

Methods

Collection of Spatially Mapped Samples and 3D Modeling

Neurosurgeons carefully collected samples throughout the surgical resection using a pituitary rongeur (75–225 mg). The intraoperative location of each tumor sample was recorded using a set of LPS (left, posterior, superior) coordinates mapped back to a preoperative magnetic resonance image (MRI) using a Brainlab pointer and Brainlab Cranial Navigation software (v3; BrainLAB AG). Using these coordinates and the preoperative MRI, a 3D spatial map was constructed for each tumor. The use of these patient samples was approved by the University of California Committee on Human Research. Informed consent was given by all patients.

Sample Allocation

A UCSF Brain Tumor Center Biorepository staff member was present in the operating room to acquire blood from existing lines prior to skull opening and for tissue acquisition following strict standard operating procedures to optimally preserve the biospecimen. For each sample, size permitting, 2/3 was flash-frozen in liquid nitrogen for DNA + RNA extraction and sequencing, and 1/3 was placed in 10% neutral-buffered formalin (8–14 h), processed, and paraffin-embedded, creating formalin-fixed paraffin-embedded (FFPE) blocks.

3D Modeling

Image registration was performed to the preoperation T_1-weighted postgadolinium series using FLIRT (FMRIB's Linear Image Registration Tool) package.[30,31] Brain extraction from the T_2-weighted FLAIR image stack was performed using FSL's BET.[32] Volumetric tumor ROIs were drawn for each tumor from the T_2-weighted hyperintense region and from contrast-enhancing lesions. Spherical ROIs (5 mm) were generated for each sample coordinate and converted to DICOM format for visualization and downstream analysis. DICOM files corresponding to the extracted brain, tumor ROIs, and sample ROIs were imported into freely available software Slicer.[33] Volumetric 3D models of the brain, tumor, and sample ROIs were generated using Slicer's Grayscale Model Maker module.

DNA and RNA Isolation

See Supplementary Methods for details.

Whole Exome Sequencing and Copy-number Analysis

The Nimblegen SeqCap EZ Exome v3 kit (Roche), the SureSelect Human All Exon V5 kit (Agilent Technologies),

and the xGen Exome Research Panel v2 (Integrated DNA (IDT) Technologies) were used according to the manufacturer's protocol (Supplementary Table S1). Sequencing was performed on a HiSeq2000, HiSeq4000, or NovaSeq (Illumina).

Exome data were processed as previously described.[34] FACETS[35] was used to estimate the copy number across chromosomes. FACETS estimates of total copy number were used to identify oncogene amplification events. Samples with very low tumor purity and no detectable amplification were considered indeterminate in assessing amplification heterogeneity. The genome build hg19 was used for all sequencing data alignment. Exome data is deposited at EGA (EGAS00001003710).

Tumor Purity Estimates

Tumor purity (percent of tumor to nontumor cells) was estimated from exome sequencing using FACETS.[35] Samples with very low tumor purity were assigned a value of NA (not measurable), indicating that tumor purity was too low to estimate.

RNAseq Data Processing

The KAPA Stranded mRNA-Seq Kit (KR0960-v2.14, Kapa Biosystems) was used to prepare strand-specific transcriptome sequencing libraries. TopHat (v2.0.12: P41; v2.0.14: P302–P373, P450–P481; v2.1.1: P413, P485–P522) was used to align transcriptome sequencing data to the hg19 reference genome using a GENCODE V19 transcriptome-guided alignment and then processed through custom quality-control scripts as previously described.[36] The number of reads per gene was calculated by featureCounts (v1.4.6, standalone version).[37] RNA-seq results are expressed as transcripts per million. RNA-seq data are deposited at EGA (EGAS00001003710).

Polymerase Chain Reaction (PCR)

PCR was performed using the Thermo Scientific Phusion High Fidelity PCR kit. Regions containing the following sites were amplified: the G228A or G250A-TPM site; the *IDH1* mutation site; and common SNPs on chromosome 10 that were found to be heterozygous in our patients (*LIPA*, *LIPK*, or *MMRN2*) (to assess chromosome 10 loss). Partial Illumina adapters were added to the 5′ end of both the forward and the reverse primer. PCR products were purified with the Zymo DNA Clean and Concentrator-5 kit. See Supplementary Methods for details of PCR conditions.

Sanger Sequencing

TPM variant status was assessed by Sanger sequencing performed in both the forward and reverse direction. The traces were analyzed for a distinct G228A or G250A peak and the result was recorded. See Supplementary Methods for details.

Deep Amplicon Sequencing (AmpSeq)

The concentration of DNA samples on which AmpSeq was performed was determined by Qubit. AmpSeq was performed on 208 samples, including 190 tumor samples and 18 patient-matched whole blood samples (Genewiz, Amplicon-EZ). *TERT* and *IDH1* amplicons were combined in equimolar amounts into one tube for each OD sample. For each GBM sample, amplicons for *TERT* and a chromosome 10 SNP (*LIPA*, *LIPK*, or *MMRN2*) were combined in equimolar amounts into one tube. Amplicons were sequenced using the Illumina MiSeq paired-end protocol with 250 bp read length.

Controls for AmpSeq

See Supplementary Methods for details.

AmpSeq Alignment and Variant Calling

Raw fastq files were aligned to the hg38 genome using minimap2 v.2.17.[38] Obtained SAM files were converted to BAM, sorted, and indexed using samtools v.1.7.[39] Allele coverage of the locations of interest were extracted from the samtools mpileup output using a custom Python script. A sample was deemed positive for a variant if the VAF was greater than 2 standard deviations from the mean of the VAF of that variant in the whole blood sample combined with the mean of the VAF of the negative control (*IDH*-mutant grade 4 astrocytoma; Supplementary Table S2).

UCSF500 and MSK-IMPACT NGS Data

The UCSF500 NGS Panel is a sequencing assay that targets 479 genes related to human cancer. For OD, the dataset was obtained by accessing a private cBioPortal instance available to UCSF clinicians, researchers, and staff. Meanwhile, the MSK-IMPACT glioma dataset was obtained from cBioportal. We filtered both datasets to include only cases diagnosed as OD with an *IDH1* R132H mutation and a hotspot TPM (C228T or C250T).

For GBM, data were also obtained from the UCSF500 NGS panel. The TPM VAF was recorded, along with the VAFs at 11 common single nucleotide polymorphisms (SNPs) on chromosome 10, when informative, by direct inspection of sequencing data in the Integrative Genome Viewer (IGV). GBM lacking canonical TPM, harboring copy number imbalance of chromosome 5p including the *TERT* locus, or lacking monosomy or loss of heterozygosity of chromosome 10q were excluded, based on inspection of chromosomal copy number and zygosity plots generated by CNVkit and visualized using NxClinical (Biodiscovery). For comparing VAFs, we generated graphs for OD and GBM using ggplot2 in R studio.

RNAscope

FFPE sections were evaluated by RNAscope chromogenic in situ hybridization (CISH) assay for the expression of *TERT*

using Advanced Cell Diagnostics (ACD) probes (Newark, CA) specific for *TERT* mRNA. The RNA Probe PPIB and dapB were used as positive and negative control probes, respectively. The RNAscope CISH assays were performed using the Ventana Discovery platform according to the automated RNAscope protocol optimized for use on the instrument. Chromogenic detection was performed using the Roche mRNA DAB Detection kit. The slides were counterstained with hematoxylin and slides were imaged at 40×. RNAscope was considered positive for *TERT* expression if greater than one cell was positive in a high power (40×) field.

RNA scope slides were analyzed using QuPath version 0.2.3. An area of 100 cells minimum was selected for quantification. The requested pixel size was set to 0.5 μm. The maximum area was set to 80 μm^2. For each sample, the total number of nuclei, nuclei positive for mRNA, and total number of discrete probe signals corresponding to *TERT* mRNA were counted. Positive and negative control FFPE samples were included in each run.

Histologic Evaluation of Hematoxylin and Eosin (H&E)-Stained Slides:

H&E-staining of tissue sections adjacent to those analyzed by RNAscope were evaluated for tumor cells (tumor purity), necrosis, microvascular proliferation, and abundance of perivascular lymphocytes. Histologic features were recorded as present or absent and were also scored as follows: necrosis: 1–10% (1+), 11–20% (2+), >20% (3+); microvascular proliferation: 1–9% (1+), 10–14% (2+), >15% (3+); and perivascular lymphocytes: sparse (1+), moderate (2+), and abundant (3+).

Statistical Analysis

Pearson correlation coefficients were calculated to assess the strength of all correlations except for *TERT* expression (by RNA-seq) with tumor purity and with TPM VAF, which were calculated using Spearman correlation.

Results

Maximal Intratumor Sampling Approach

We developed a 3D maximal sampling approach to determine clonality and intratumoral heterogeneity of genetic events on whole tumors and applied this to our study of TPM clonality (Figure 1A–C). Our cohort is composed of 19 GBM and 10 OD from which a total of 271 tumor samples were obtained, along with 28 patient-matched whole blood samples (Table 1). Additionally, 8 samples from an *IDH*-mutant grade 4 astrocytoma (P33) were included as a negative control (Supplementary Table S2). Exome sequencing was previously generated for all 299 samples and RNA sequencing for 197 tumor samples. All tumor samples in the study have a 3D spatial coordinate corresponding to the tumor region they represent (Figure 1A and B), with approximately 9 samples per tumor on average (Supplementary Table S4). One patient (P516) had 2 adjacent tumors, an *IDH*-mutant, 1p/19q codeleted OD, and an *IDH*-mutant, 1p/19q intact astrocytoma which had 7 samples that were not studied further, bringing the total tumor sample count to 264. The GBM are *IDH*-wildtype and 16 of 19 have chromosome 7 gain and chromosome 10 loss (Supplementary Table S5). Three GBM have either chromosome 7 gain or chromosome 10 loss (Supplementary Table S5) but met histological criteria for the diagnosis of GBM (microvascular proliferation and/or necrosis). The OD are *IDH*-mutant and 1p/19q codeleted (Supplementary Table S5). Here we apply the whole tumor sampling approach to determine the evolutionary timing of TPM and to investigate the relationship between TPM and *TERT* expression at the highest possible resolution (Figure 1C).

Clonality of TPM on a Tumor-Wide Scale

Detection of TPM in all samples from a maximally sampled tumor would strongly suggest a very early origin and clonality on a tumor-wide scale. In contrast, the absence of TPM in even 1 sample in which other alterations are detected would support subclonality and a later origin. As an initial, rapid screen, high-specificity but low-sensitivity Sanger sequencing was performed on PCR products from all 264 tumor samples and 28 patient-matched whole blood samples (Table 1). A heterozygous G228A TPM was found in 22 tumors and a heterozygous G250A TPM was found in 7 tumors (Table 1). A visually distinct peak at either of the canonical TPM locations was detected in 226 of 264 samples (85.6%; Supplementary Table S6). Samples with an estimated tumor purity of 31.7% or greater were positive for TPM. Furthermore, TPM was identified in samples with tumor purity as low as 21.4% (Supplementary Tables S7 and S8). Tumor purity estimates for GBM ranged from 18.9% to 94.0% (average 64.5%; Supplementary Table S7). Tumor purity estimates for OD ranged from 24.6% to 96.8% (average 75.1%; Supplementary Table S8). Of the 39 tumor samples with unmeasurable tumor purity TPM was nevertheless detected by Sanger sequencing in 5 samples (12.8%; Supplementary Tables S9 and S10). Traces for tumor samples on which only Sanger sequencing was performed are shown in Supplementary Figure S2. From these binary Sanger sequencing calls alone, it is unclear if the 38 samples that are TPM-negative lack tumor cells, or whether tumor cells are present but lack TPM.

To definitively determine the presence or absence of TPM and to compare the frequency of TPM with that of alterations that occur early in tumor evolution, we performed a quantitative, high-sensitivity assay, deep amplicon sequencing (AmpSeq, average sequencing depth 59,473X), on a total of 187 samples from 21 tumors. Tumors that had at least 1 sample negative for TPM by Sanger sequencing were included, along with many other GBM and OD.

TPM was present in 181 of 187 (96.8%) tumor samples (Supplementary Table S6). The remaining 6 samples were from the group of 39 samples in which tumor was not detected (Supplementary Tables S9 and S10). TPM VAF for GBM ranged from 10.8% to 79.8% (average 49.1%; Supplementary Table S7) while TPM VAF for OD ranged from 12.0% to 74.6% (average 52.2%; Supplementary Table S8). Thus, TPM is readily detectable in 258 of 264

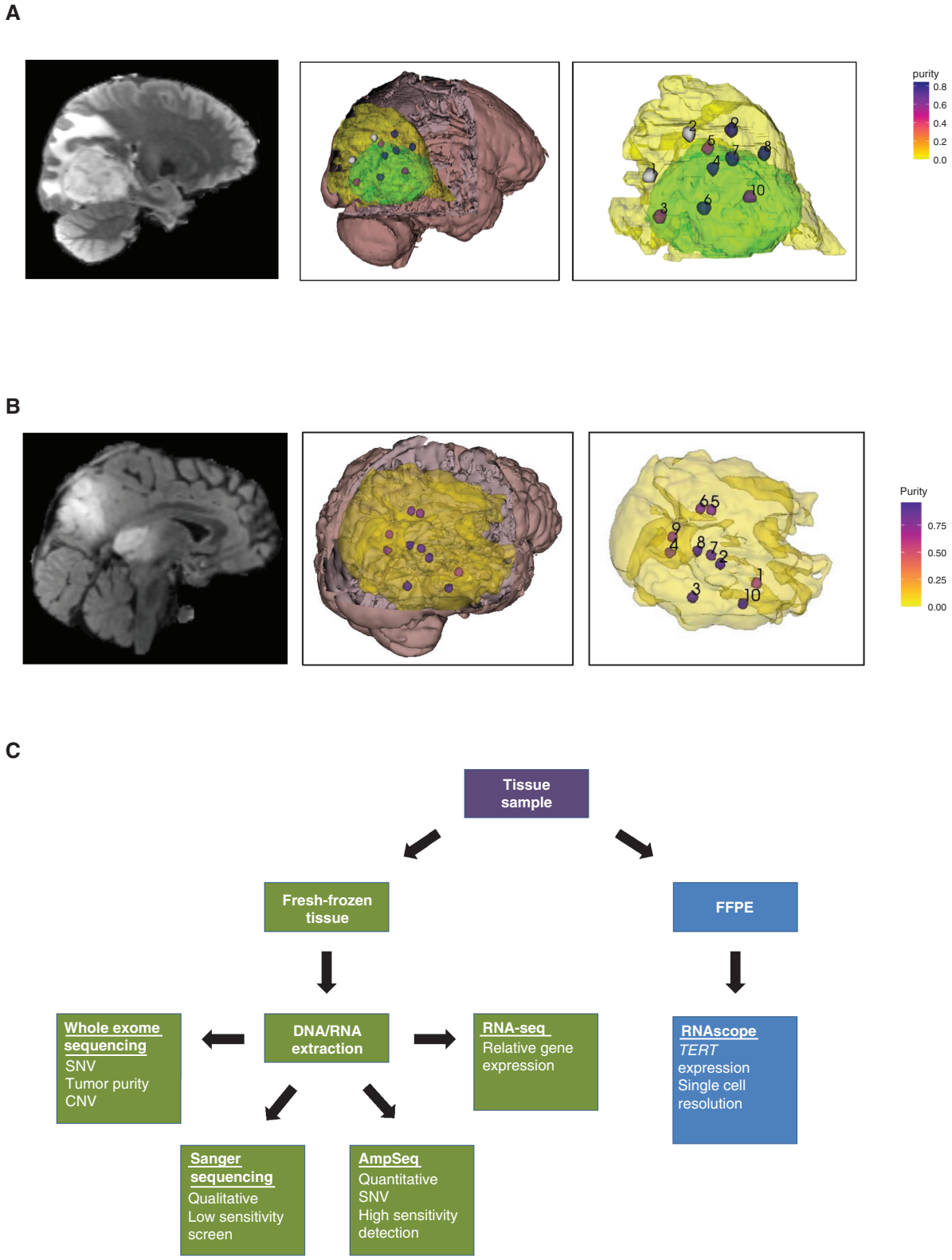

Figure 1. Spatial mapping approach and experimental workflow. (A and B) 3D models are constructed based on the patient's preoperative MRI (left). Models of a GBM (P503) (A) and an OD (P450) (B) are shown, indicating the intraoperatively determined 3D spatial locations of the 10 regions that were sampled. The green shading (A) represents the area of contrast enhancement and the yellow shading (A and B) represents T2 enhancement. The samples in the 3D model are shaded by tumor purity (gradient key, 1.0 equals 100% tumor) estimated from exome sequencing. Gray shading indicates very low tumor purity samples (assigned value of NA by FACETS). (C) Schematic of experimental workflow. seq = sequencing, AmpSeq = Amplicon sequencing.

Table 1. Cohort of Spatially Mapped Samples from Glioblastoma (GBM) and Oligodendroglioma (OD)

Tumor Type	Number of Tumors (29)	Tumors with C228T (22)	Tumors with C250T (7)
Primary GBM	15	11	4
Recurrent GBM	4	3	1
Primary OD	4	3	1
Recurrent OD	6	5	1
Sequencing Assay	**Number of Samples (299)**	**Tumor Samples (271)**	**Matched Blood Samples (28)**
Sanger	299	271	28
AmpSeq	205	187	18
Exome	299	271	28
RNA-seq	197	197	NA

Abbreviations: GBM = glioblastoma, OD = oligodendroglioma, Sanger = Sanger sequencing, AmpSeq = amplicon sequencing, Exome = whole exome sequencing, RNA-seq = RNA sequencing.

tumor samples, or 97.7% of the entire sample cohort using Sanger sequencing and a sensitive deep sequencing assay. TPM was not detected in 6 samples, mostly obtained from the tumor periphery or beyond, but tumor cells were also not detectable by FACETS.

In addition, 2 samples (P481-10, P503-1) that were negative for TPM by Sanger sequencing did not have sufficient DNA remaining for AmpSeq; however, tumor cells were not detectable in these samples and no copy number changes or driver mutations were found by whole exome sequencing. The data support a tumor-wide presence of TPM in GBM and OD.

We next sought to determine whether TPM is clonal within each sample by comparing the VAF of TPM to that of presumed early, clonal events. A common SNP on chromosome 10 (*LIPA*, *LIPK*, or *MMRN2*) was used to estimate clonality of chromosome 10 loss, an alteration that is considered clonal in GBM.[27,40] Chromosome 10 SNP VAF for GBM in which both TPM and chromosome 10 loss were identified ranged from 54.4% to 98.7% (average 80.8%; Supplementary Table S7). *IDH1* mutation VAF in OD ranged from 10.6% to 55.5% (average 41.3%; Supplementary Table S8).

Not only was TPM present in each sample with measurable tumor purity, the VAF of TPM was equivalent to that of other presumed clonal alterations. In GBM, chromosome 10 SNP VAF showed a high positive correlation with tumor purity ($R = 0.97$, $P < .0001$) (Figure 2A). Likewise, TPM VAF showed a high positive correlation with chromosome 10 SNP VAF in GBM ($R = 0.85$, $P < .0001$; Figure 2B) and with tumor purity ($R = 0.91$, $< .0001$; Figure 2C). In OD, *IDH1* mutation VAF showed a high positive correlation with tumor purity ($R = 0.88$, $P < .0001$; Figure 2D). Three OD samples from P302 (#2, 6, 11) had a higher *IDH1* mutation VAF than expected given the tumor purity (Figure 2D). Copy number plots for these samples showed gains of multiple chromosomes, including chromosome 2 which contains *IDH1* (Supplementary Figure S3A, B, and E), possibly accounting for the higher *IDH1* mutation VAF. TPM VAF showed a high positive correlation with *IDH1* mutation VAF ($R = 0.87$, $P < .0001$; Figure 2E) and tumor purity in OD ($R = 0.9$, $P < .0001$; Figure 2F). Of the 39 samples in which tumor cells could not be detected, TPM was found in 33 (84.6%). These samples also showed a positive correlation between TPM and clonal alterations in both GBM and OD (Supplementary Figure S4A and B). No copy number changes or other driver mutations could be detected by exome sequencing or AmpSeq (chromosome 10 loss, *IDH1* mutation) in the 6 TPM-negative samples. Taken together, these results suggest TPM is present throughout the tumor and in most if not all tumor cells.

For comparison in evolutionary timing, we analyzed driver oncogene amplifications in 186 samples from 19 GBM (Figure 3, Supplementary Table S11). We identified amplifications in *EGFR*, *PDGFRA*, *MYCN*, and *MDM4*, all of which were also detected in multiple samples with low tumor purity, some of which were strikingly high (Figure 3, Supplementary Table S11). Oncogene amplification was observed tumor-wide in 12 cases and heterogeneously for *PDGFRA* in 2 of 2 tumors, for *MYCN* (1 tumor) and for *EGFR* in 2 of 9 tumors (Figure 3, Supplementary Table S11). Therefore, amplification and TPM occur at roughly similar evolutionary time points in most patients, but occasionally TPM precedes amplification.

Analysis of additional genomic datasets supports our findings with TPM. Chromosome 10 SNP VAF showed a strong positive correlation with TPM VAF in single samples from 100 consecutive GBM assayed by the UCSF500 clinical sequencing panel (Supplementary Figure S6A, Table S12). *IDH1* mutation VAF showed a significant positive correlation with TPM VAF in OD from 2 independent datasets, including single samples from 53 tumors assayed by the UCSF500 clinical sequencing panel and 105 tumors from the MSK-IMPACT cancer gene panel. The correlations among OD samples were moderately lower than in our cohort (Supplementary Figure S6B and C). These clinical sequencing assays are performed on FFPE whereas our intratumor samples are fresh frozen tissue which may contribute to differences. There is also substantially reduced genetic variation among intratumoral samples compared to variation among patients.

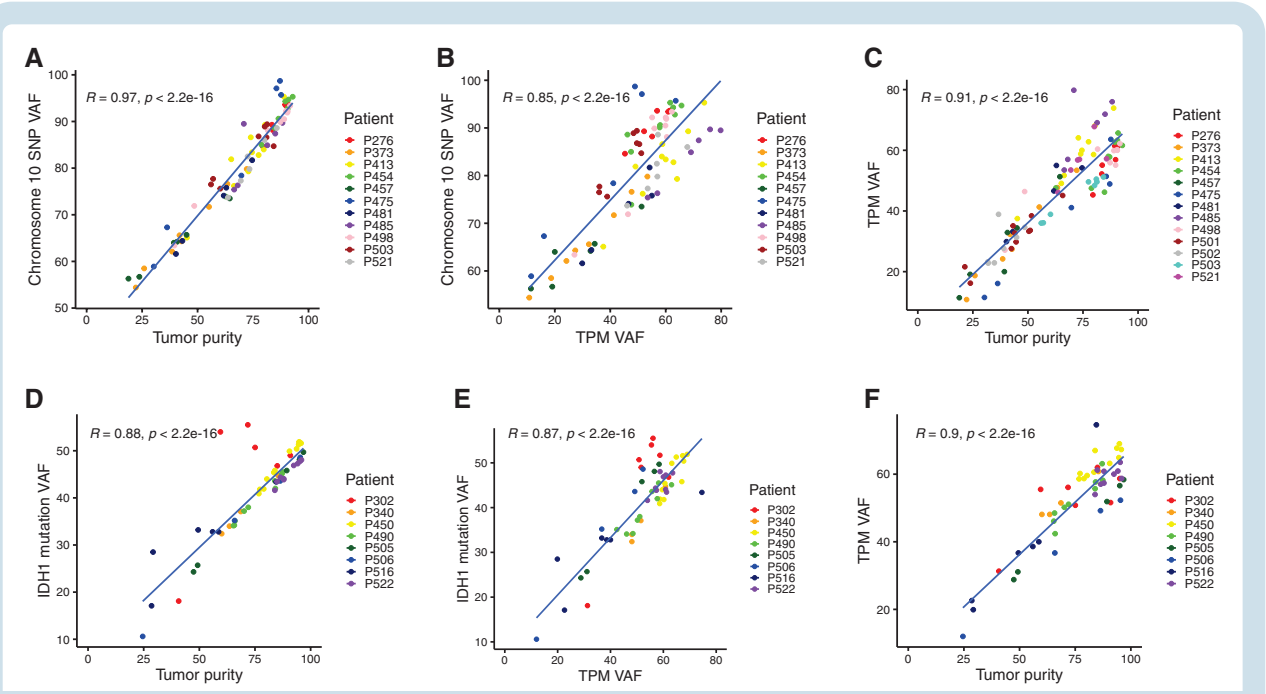

Figure 2. Correlation of the *TERT* promoter mutation (TPM) with putative clonal alterations and tumor purity. Scatter plots showing pairwise comparisons between chromosome 10 SNP VAF and tumor purity (A), chromosome 10 SNP VAF and TPM VAF (B), and TPM VAF and tumor purity (C) in GBM and *IDH1* mutation VAF and tumor purity (D), *IDH1* mutation VAF and TPM VAF (E), and TPM VAF and tumor purity (F) in OD. The dots are colored by patient number. The Pearson correlation coefficient is noted on each graph to signify the strength of each correlation. Tumor purity is estimated from whole exome sequencing and expressed as the percentage of tumor cells present. For graphs A and B, all samples from 2 patients' tumors (P501 and P502) were omitted because they did not show clonal chromosome 10 loss in the region of the SNPs.

Relationship of *TERT* Expression to TPM and Tumor Purity

As TPM and *TERT* expression are mostly, if not entirely, tumor-specific, a positive correlation might be expected between *TERT* expression and TPM VAF and between *TERT* expression and tumor purity. *TERT* expression, however, showed only a moderate positive correlation with tumor purity in GBM ($R = 0.56$, $P < .0001$; Figure 4A) and OD ($R = 0.64$, $P < .0001$; Figure 4C). *TERT* expression also showed a moderate positive correlation with TPM VAF in both GBM ($R = 0.52$, $P < .0001$; Figure 4B) and OD ($R = 0.65$, $P < .0001$; Figure 4D). Three GBM samples from P475 (#2, 3, and 6) had higher *TERT* expression than expected given the tumor purity and TPM VAF (Figure 4A and B). Copy number plots for these samples showed gains of multiple chromosomes, including chromosome 5 which contains *TERT* (Supplementary Figures S5A–C), which may contribute to their higher *TERT* expression. Furthermore, in OD the relationships between *TERT* expression and tumor purity (Figure 4C) and *TERT* expression and TPM VAF were nonlinear (Figure 4D) suggesting additional variables influence *TERT* expression level. In comparison, *IDH1* expression from the mutant allele in OD had a more linear relationship to tumor purity and to *IDH1* mutation VAF (Figures 4E and F). Furthermore, mutant *IDH1* expression is detectable at the protein level in most if not all *IDH*-mutant tumor cells in situ.[41–43] Like *TERT*, however, mutant *IDH1* expression can be influenced by other variables in addition to *IDH1* mutation VAF. Five samples from P302 had higher mutant *IDH1* expression than expected from the tumor purity (Figure 4E). All these samples showed a gain in the copy number of chromosome 2 and other chromosomes (Figures S3A–E). Though most of these samples also had a higher *IDH1* mutant VAF, 1 sample (#7) had higher mutant *IDH1* expression than expected from either tumor purity or *IDH1* mutant VAF (Figure 4E and F). Three samples from P340 had lower mutant *IDH1* expression than expected from either tumor purity or *IDH1* mutant VAF (Figures 4E and F), however, no copy number changes are seen in the chromosomal region of *IDH1* for these samples (data not shown).

Intercellular Heterogeneity of *TERT* Expression

The lower-than-expected correlations between TPM VAF and *TERT* expression suggest the relationship may be more complex than the relationship between *IDH1* mutation and *IDH1* expression. This raises new questions about the regulation of the mutant *TERT* promoter in tumor cells in vivo, prompting us to re-examine *TERT* expression at the highest possible resolution. RNAscope is an in situ hybridization method that detects gene expression at the single-cell level in FFPE tissue, including low-abundance transcripts like *TERT*.[12,44] We initially examined *TERT* expression in 4 GBM and 4 OD, with an average of 6 spatially distinct samples per tumor. Inspection of scanned images showed that *TERT* mRNA has mostly nuclear or perinuclear localization[45] (Figure 5A). RNAscope data

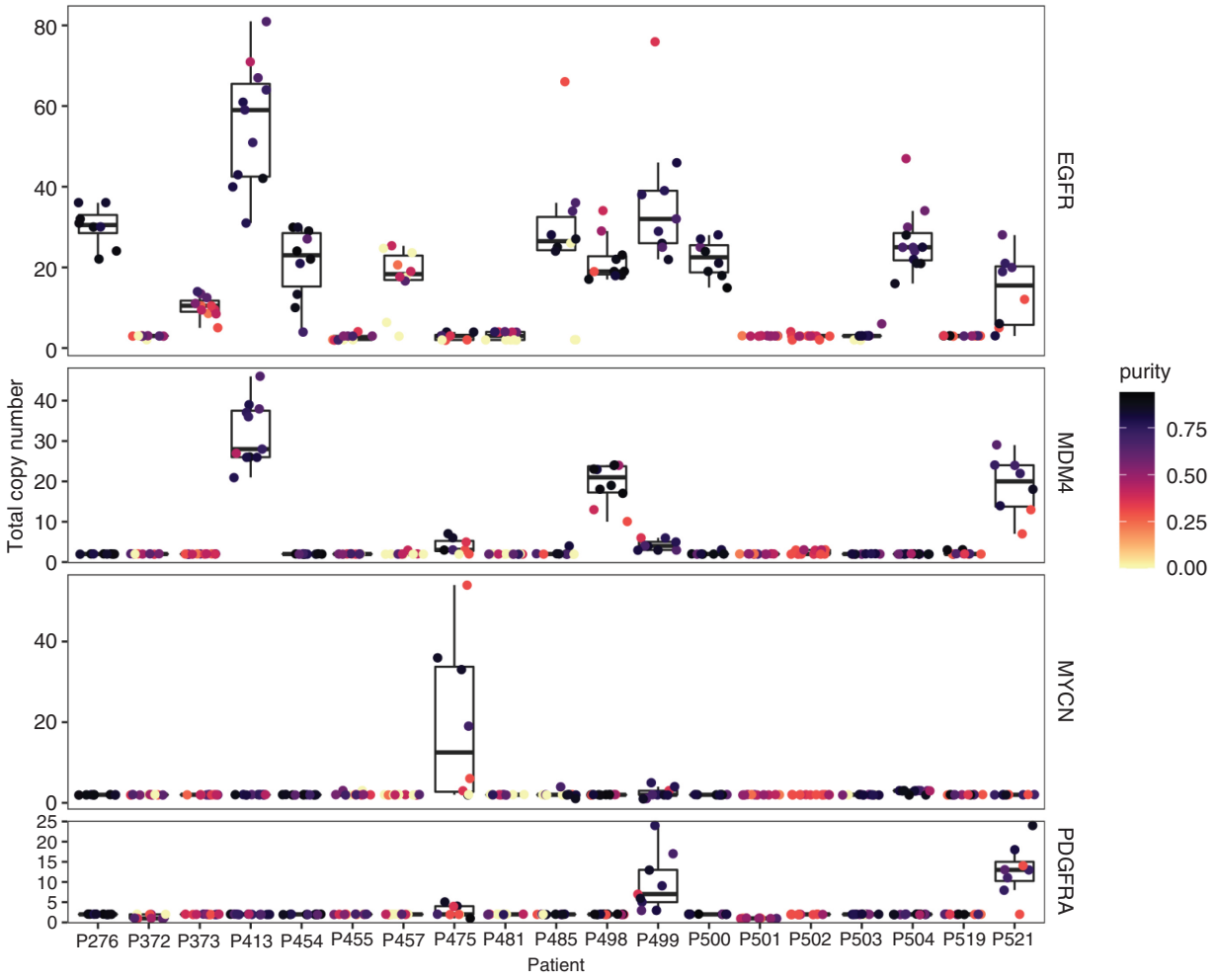

Figure 3. Whole tumor analyses of *EGFR, MDM4, MYCN,* and *PDGFRA* amplification in 19 GBM. Box plots showing distribution of *EGFR, MDM4, MYCN,* and *PDGFRA* copy number of each sample (dots) for all GBM. Dots are shaded by tumor purity value. Copy number and tumor purity are estimated from whole exome sequencing.

were analyzed by dividing the number of positive cells over the number of all cells present and also by dividing the total number of probes by the number of all positive cells to calculate the average number of probes in each *TERT*-positive cell. Unlike the *TERT* promoter mutation, which was seen throughout the entire tumor, *TERT* expression was detected only in a subset of cells in GBM and in OD (Figures 5A–C). The average number of probes per positive cell ranged from 1.0 to 5.6 (average 2.2) for GBM (Supplementary Table S13) and 0–4.1 (average 2.6) for OD (Supplementary Table S14). The percentage of positive cells ranged from 0.6% to 79.9% (average 33.5%) for GBM (Supplementary Table S13) and 7.2–59.5% (average 26.5%) for OD (Supplementary Table S14). A moderate negative correlation was seen when comparing *TERT* expression by average number of probes per positive cell and *TERT* expression by percentage of positive cells in both tumor subtypes (Figures 5B and C). When comparing *TERT* expression with tumor purity, modest negative correlations were seen between average number of probes per positive cell and tumor purity (both by FACETS and by histologic assessment) in OD and moderate positive correlation was seen between the percent of positive cells and histologic tumor purity estimates (Supplementary Figure S7). We tested for but did not detect a correlation between *TERT* expression and tumor purity in GBMs; *TERT* expression and histologic features in GBM; or *TERT* expression and RNA-seq results in GBM or OD.

To begin to address the clinical utility of *TERT* expression, we examined an additional 10 *IDH*-wildtype GBM, 2 *IDH*-mutant OD, 2 *IDH*-mutant astrocytomas, and 1 case of subpial and subcortical gliosis. The latter 3 cases were negative for *TERT* expression supporting specificity of the assay for tumors that express *TERT*. The other 12 cases were positive for *TERT* expression (Supplementary Table S15). Given the specificity, we reasoned that this assay may be able to detect tumor cells in equivocal samples. Therefore, we performed RNAscope on 10 samples with low tumor purity, including both GBM and OD, ranging from 0% to 40% tumor purity by histologic assessment

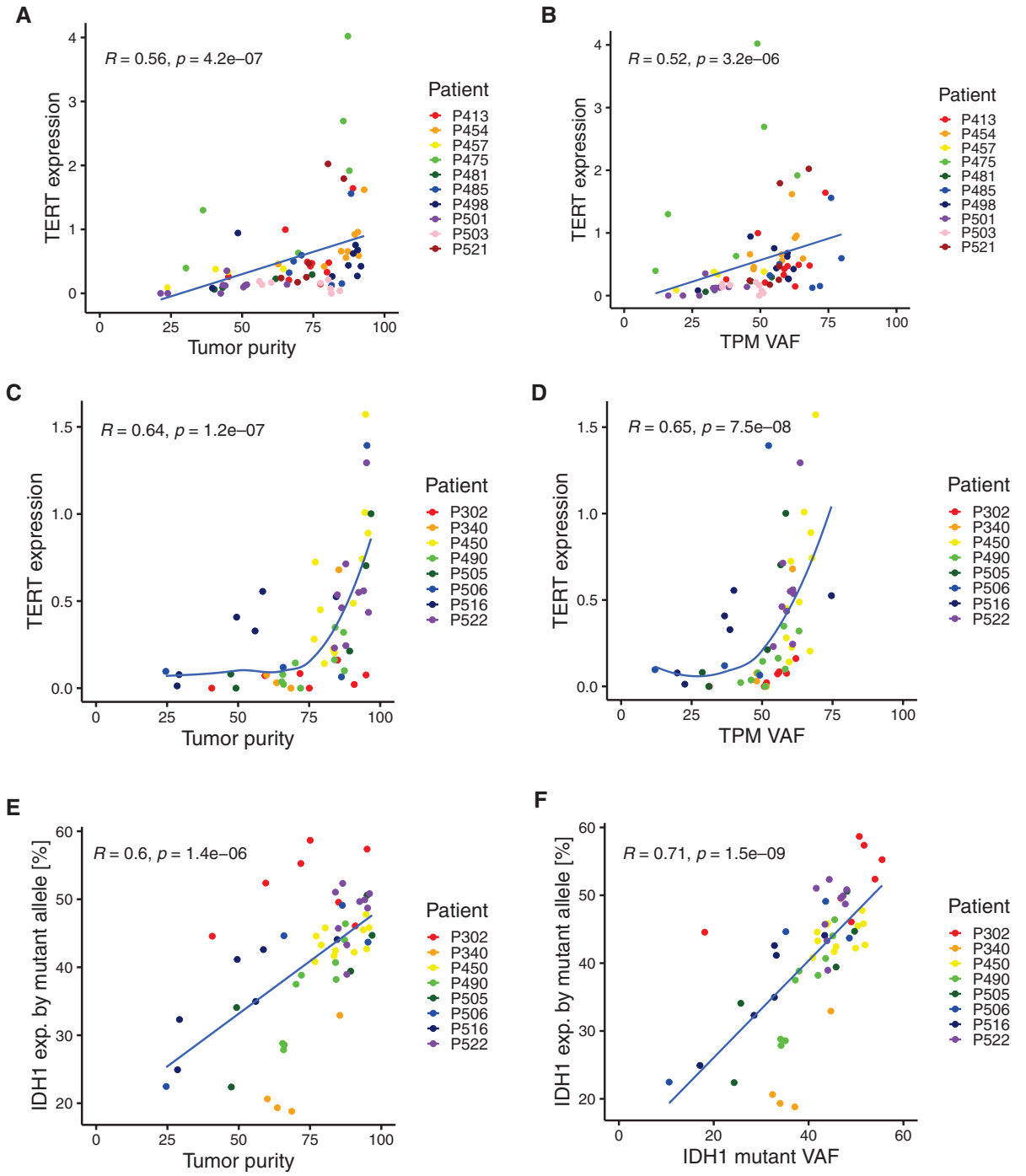

Figure 4. Correlation of *TERT* and *IDH1* expression with tumor purity and with *TERT* promoter mutation (TPM) and *IDH1* mutation, respectively. Scatter plots showing pairwise comparisons of *TERT* expression and tumor purity and *TERT* expression and TPM VAF for both GBM (A and B, respectively) and OD (C and D, respectively). Scatter plots showing pairwise comparisons between *IDH1* expression (by percent mutant allele) and tumor purity (E) and *IDH1* mutation VAF (F) for OD. The dots are colored by patient number. The Spearman correlation coefficient is noted on each graph to signify the strength of each correlation. Tumor purity is estimated from whole exome sequencing and is expressed as the percentage of tumor cells present. *TERT* expression is expressed in transcripts per million.

(Supplementary Table S16). We also performed RNAscope on an *IDH*-wildtype GBM that showed no histologic features of GBM but was later found to have molecular alterations of *IDH*-wildtype GBM by NGS (Supplementary Table S15). All 11 cases were positive for *TERT* expression (Supplementary Figure S8, Tables S15 and S16). For OD samples with lower purity, immunohistochemistry for IDH1 R132H was performed on adjacent sections, to

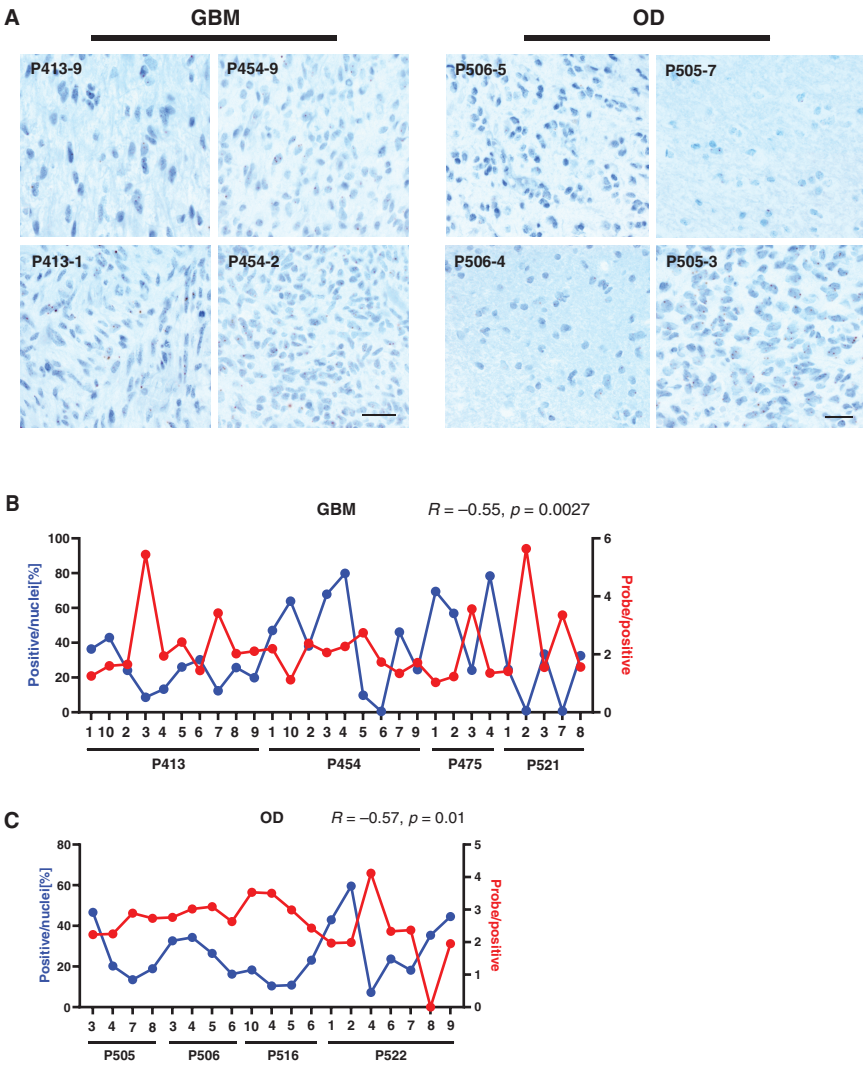

Figure 5. Detection of *TERT* expression at the single-cell level by RNAscope. (A) *TERT* expression by RNAscope in 2 GBM (left) and 2 OD (right). Each image is labeled with the patient number and sample number (upper left of image). Variation of *TERT* expression is shown both for GBM (B) and OD (C). Quantification of *TERT* expression is expressed by the total number of probes divided by the number of positive cells (probe/positive) and by the number of positive cells divided by the total number of cells (positive/nuclei [%]) for both GBM and OD. Scale bars denote 10 μm.

identify tumor cells in each sample (Supplementary Table S16). Two OD samples were negative for IDH1 R132H immunostaining but were positive for *TERT* expression. As these samples were on the same slide, this could represent a false negative and likely does not indicate complete absence of tumor cells. These results provide preliminary evidence of the clinical utility of the assay for *TERT* mRNA and promote follow-up analyses in larger cohorts.

Discussion

Although previous studies have addressed TPM clonality in gliomas,[25–29] single samples were predominantly used, leaving open the question of its timing in tumor evolution and ultimately the value as a therapeutic target. In 1 notable exception, whole exome sequencing and targeted deep sequencing on grades 2 and 3 OD showed that *IDH* mutation, *TERT* promoter mutation, and codeletion of 1p/19q were truncal events and approximately concurrent in 6 cases with multi-sampling.[29] In 10 newly diagnosed *IDH*-wildtype GBM with biopsies from 2 regions ($n = 9$) or 4 regions ($n = 1$), and deep sequencing (average coverage 4680X), TPM was the only mutation consistently detected in each region, suggesting clonality.[28] In contrast, other studies suggest TPM is subclonal, including a rigorous study of whole genome sequencing on 21 pairs of primary and recurrent *IDH*-wildtype GBM (single sample per tumor) and deeper NGS on 43 pairs of primary and recurrent *IDH*-wildtype GBM. TPM was present in all pairs, except for 1 primary tumor, but it was determined to be subclonal in 33% of the tumors, though the VAF of TPM was significantly higher than other subclonal

mutations.[27] In another study, targeted NGS on 176 pairs of primary and recurrent *IDH*-wildtype GBM from patients treated with chemoradiotherapy used SNaPshot analysis of TPM. Thirteen (12.4%) tumors lost TPM at recurrence and 1 tumor that was initially TPM-negative gained TPM at recurrence.[26] Another study used whole exome sequencing on 12 GBM pairs along with a Fluidigm PCR assay followed by NGS for targeted sequencing of *TERT*. The 12 GBM pairs contained 1 sample per tumor as follows: pretreatment primary tumor and posttreatment autopsy brain (9 pairs), recurrent tumor and posttreatment autopsy brain (1 pair), and posttreatment autopsy brain and metastasis (2 pairs). Of the 9 pairs with pretreatment tumor and posttreatment autopsy brain, 7 pairs had TPM status available for both pretreatment and posttreatment samples. TPM was clonal in 6 pairs (86%) for both sets of samples while it was subclonal in the pretreatment sample and clonal in the posttreatment sample for 1 pair (14%). TPM was clonal in all other samples except 4 samples with no *TERT* promoter status available.[25]

Potential explanations for the conflicting conclusions[25–29] center primarily on tumor purity,[46] sequencing depth, and extent of sampling. In addition, the different approaches to estimating tumor purity, including multiple computational methods and histological assessment by a pathologist,[35,47,48] may influence the results. Different assays were used to assess TPM in these studies, and the sequencing depth varied considerably.

Through maximal sampling, we find that TPM is present throughout each tumor, and in most if not all tumor cells, defining TPM as one of the earliest events in the evolution of GBM and OD. By accounting for tumor purity, we avoid false negatives that have the potential to erroneously suggest subclonality. Thus, therapy targeted against TPM-positive cells could theoretically affect the entire tumor. However, unlike TPM, *TERT* expression shows intercellular variability, a pattern also reported in vitro.[45] This could in part explain why *TERT* expression is relatively low in GBM and OD compared to most other genes. The intercellular variability also raises interesting questions regarding *TERT* regulation. We cannot, however, rule out the possibility that cells lacking detectable *TERT* mRNA are false negatives in the RNAscope assay because *TERT* expression is low compared to other genes. On the other hand, the assay shows potential for clinical use as all samples with TPM were positive, including samples with lower tumor purity, and samples without TPM were negative suggesting specificity.

Our study of TPM clonality is unique in that all tumor samples in the study are spatially mapped. Not only are there multiple samples for each tumor but also more importantly, each tumor is maximally sampled, allowing accurate and comprehensive characterization of TPM. Instead of inferring clonality based on 1 sample, comprehensive sampling allows for a robust and definitive assessment. Furthermore, chromosome 10 loss and *IDH1* mutation are assessed for each sample in GBM and OD, respectively, and compared directly with TPM using the same assay.

While our study assesses TPM clonality in relation to other driver events in a novel way, it also has limitations. Although TPM is typically a heterozygous mutation, a subset of samples exhibited a VAF higher than 50%. There are also samples that have a TPM VAF that is higher than expected based on tumor purity. While copy number changes in the region of TPM might explain these results, our copy number plots do not show changes at the *TERT* locus. A slight bias favoring the mutant allele during PCR might also contribute, as suggested by the Sanger sequencing traces which correlate well with the VAF. For these reasons, it is not possible for us to determine whether TPM occurs asynchronously or concurrently with other early events in GBM and OD.

Targeting TPM-positive cells is an important clinical goal with the potential for cancer-cell specificity,[49] sparing normal cells. Determining if TPM is clonal on a tumor-wide scale is the first step in exploring TPM-positive cells as possible targets. Anti-tumor efficacy in targeting telomerase-positive cells has been demonstrated in preclinical studies with Clustered Regularly Interspaced Short Palindromic Repeats (CRISPR) interference knockdown of *TERT* expression in *TERT* promoter-mutant GBM cell lines and patient-derived models[50] and with the purine nucleoside analog 6-thio-2′-deoxyguanosine (6-thio-dG).[51–53] To target TPM directly, CRISPR interference and programmable base editing to revert TPM (–124 C >T) to wildtype reduced *TERT* expression and induced senescence.[54] While therapies to target the transcription factor GABP have not yet been developed, recent advances suggest "undruggable" transcription factors can be targeted.[51]

Supplementary material

Supplementary material is available online at *Neuro-Oncology* (https://academic.oup.com/neuro-oncology).

Keywords

glioblastoma | oligodendroglioma | sequencing |TERT

Conflict of interest statement

Potential conflicts of interest: J.C.: Telo Therapeutics, Inc. (Co-founder and ownership interest).

Funding

This work was supported by National Institutes of Health/National Cancer Institute [grants R01CA244838, 2P50CA097257, P01CA118816, T32CA151022, R50CA274229]; The Brain Tumor Funders Collaborative; a generous gift from the Dabbiere Family; the Panattoni Project; and The Gianne Rae Meadows Fund.

Author contributions

Conceptualization: C.L.A., J.F.C. Data curation: I.V.S. Formal analysis: C.L.A., R.M., I.V.S., A.K.S. Funding acquisition: J.F.C. Investigation: C.L.A., C.H., R.M., A.K.S., J.J.P., A.S., A.W., D.A.S. Methodology: C.L.A., J.F.C., N.O.S., S.H. Resources: C.H., A.S., M.S.B., S.M.C., J.J.P., D.A.S. Writing-original draft: C.L.A. (lead), J.F.C., A.K.S., S.H., R.M., I.V.S., D.A.S. Writing-review and editing: C.L.A. (lead), J.F.C., A.K.S., S.H.,. R.M., I.V.S., C.H., N.O.S., A.S., M.S.B., S.M.C., J.J.P., D.A.S.

Affiliations

Department of Neurological Surgery, University of California, San Francisco, California, USA (C.L.A., A.K.S., S.H., R.M., D.A.S., I.V.S., C.H., N.O.S., A.S., A.W., M.S.B., S.M.C., J.J.P., J.F.C.); Department of Neuropathology, University of Heidelberg, Institute of Pathology, Heidelberg, Germany (A.K.S.)

References

1. Blackburn EH. Telomere states and cell fates. *Nature.* 2000;408(6808):53–56.
2. Blackburn EH, Greider CW, Szostak JW. Telomeres and telomerase: the path from maize, tetrahymena and yeast to human cancer and aging. *Nat Med.* 2006;12(10):1133–1138.
3. Blasco MA. Telomeres and human disease: ageing, cancer and beyond. *Nat Rev Genet.* 2005;6(8):611–622.
4. de Lange T. Shelterin: the protein complex that shapes and safeguards human telomeres. *Genes Dev.* 2005;19(18):2100–2110.
5. Shay JW, Wright WE. Telomeres and telomerase: three decades of progress. *Nat Rev Genet.* 2019;20(5):299–309.
6. Bryan TM, Cech TR. Telomerase and the maintenance of chromosome ends. *Curr Opin Cell Biol.* 1999;11(3):318–324.
7. Bryan TM, Englezou A, Dalla-Pozza L, Dunham MA, Reddel RR. Evidence for an alternative mechanism for maintaining telomere length in human tumors and tumor-derived cell lines. *Nat Med.* 1997;3(11):1271–1274.
8. Murnane JP. Telomere dysfunction and chromosome instability. *Mutat Res.* 2012;730(1-2):28–36.
9. Shay JW, Wright WE. Senescence and immortalization: role of telomeres and telomerase. *Carcinogenesis.* 2004;26(5):867–874.
10. Bell RJ, Rube HT, Xavier-Magalhaes A, et al. Understanding TERT promoter mutations: A common path to immortality. *Mol Cancer Res.* 2016;14(4):315–323.
11. Killela PJ, Reitman ZJ, Jiao Y, et al. TERT promoter mutations occur frequently in gliomas and a subset of tumors derived from cells with low rates of self-renewal. *Proc Natl Acad Sci U S A.* 2013;110(15):6021–6026.
12. Barger CJ, Suwala AK, Soczek KM, et al. Conserved features of TERT promoter duplications reveal an activation mechanism that mimics hotspot mutations in cancer. *Nat Commun.* 2022;13(1):5430.
13. Bell RJ, Rube HT, Kreig A, et al. Cancer the transcription factor GABP selectively binds and activates the mutant TERT promoter in cancer. *Science.* 2015;348(6238):1036–1039.
14. Herquel B, Ouararhni K, Khetchoumian K, et al. Transcription cofactors TRIM24, TRIM28, and TRIM33 associate to form regulatory complexes that suppress murine hepatocellular carcinoma. *Proc Natl Acad Sci U S A.* 2011;108(20):8212–8217.
15. McKinney AM, Mathur R, Stevers NO, et al. GABP couples oncogene signaling to telomere regulation in TERT promoter mutant cancer. *Cell Rep.* 2022;40(12):111344.
16. Liu F, Hon GC, Villa GR, et al. EGFR mutation promotes glioblastoma through epigenome and transcription factor network remodeling. *Mol Cell.* 2015;60(2):307–318.
17. Li Y, Cheng HS, Chng WJ, Tergaonkar V. Activation of mutant TERT promoter by RAS-ERK signaling is a key step in malignant progression of BRAF-mutant human melanomas. *Proc Natl Acad Sci U S A.* 2016;113(50):14402–14407.
18. Bhang HE, Ruddy DA, Krishnamurthy Radhakrishna V, et al. Studying clonal dynamics in response to cancer therapy using high-complexity barcoding. *Nat Med.* 2015;21(5):440–448.
19. Gerlinger M, Rowan AJ, Horswell S, et al. Intratumor heterogeneity and branched evolution revealed by multiregion sequencing. *N Engl J Med.* 2012;366(10):883–892.
20. Juric D, Castel P, Griffith M, et al. Convergent loss of PTEN leads to clinical resistance to a PI(3)Kα inhibitor. *Nature.* 2015;518(7538):240–244.
21. Diaz LA, Jr, Williams RT, Wu J, et al. The molecular evolution of acquired resistance to targeted EGFR blockade in colorectal cancers. *Nature.* 2012;486(7404):537–540.
22. Ding L, Ley TJ, Larson DE, et al. Clonal evolution in relapsed acute myeloid leukaemia revealed by whole-genome sequencing. *Nature.* 2012;481(7382):506–510.
23. Landau DA, Carter SL, Stojanov P, et al. Evolution and impact of subclonal mutations in chronic lymphocytic leukemia. *Cell.* 2013;152(4):714–726.
24. Turke AB, Zejnullahu K, Wu YL, et al. Preexistence and clonal selection of MET amplification in EGFR mutant NSCLC. *Cancer Cell.* 2010;17(1):77–88.
25. Brastianos PK, Nayyar N, Rosebrock D, et al. Resolving the phylogenetic origin of glioblastoma via multifocal genomic analysis of pre-treatment and treatment-resistant autopsy specimens. *NPJ Precis Oncol.* 2017;1(1):33.
26. Draaisma K, Chatzipli A, Taphoorn M, et al. Molecular evolution of IDH wild-type glioblastomas treated with standard of care affects survival and design of precision medicine trials: a report from the EORTC 1542 study. *J Clin Oncol: official J Amer Soc Clin Oncol* 2020;38(1):81–99.
27. Korber V, Yang J, Barah P, et al. Evolutionary trajectories of IDH(WT) glioblastomas reveal a common path of early tumorigenesis instigated years ahead of initial diagnosis. *Cancer Cell.* 2019;35(4):692–704.e12.
28. Mahlokozera T, Vellimana AK, Li T, et al. Biological and therapeutic implications of multisector sequencing in newly diagnosed glioblastoma. *Neuro Oncol.* 2018;20(4):472–483.
29. Suzuki H, Aoki K, Chiba K, et al. Mutational landscape and clonal architecture in grade II and III gliomas. *Nat Genet.* 2015;47(5):458–468.
30. Jenkinson M, Bannister P, Brady M, Smith S. Improved optimization for the robust and accurate linear registration and motion correction of brain images. *Neuroimage.* 2002;17(2):825–841.
31. Jenkinson M, Smith S. A global optimisation method for robust affine registration of brain images. *Med Image Anal.* 2001;5(2):143–156.
32. Smith SM. Fast robust automated brain extraction. *Hum Brain Mapp.* 2002;17(3):143–155.
33. Fedorov A, Beichel R, Kalpathy-Cramer J, et al. 3D Slicer as an image computing platform for the quantitative imaging network. *Magn Reson Imaging.* 2012;30(9):1323–1341.
34. Johnson BE, Mazor T, Hong C, et al. Mutational analysis reveals the origin and therapy-driven evolution of recurrent glioma. *Science.* 2014;343(6167):189–193.
35. Shen R, Seshan VE. FACETS: allele-specific copy number and clonal heterogeneity analysis tool for high-throughput DNA sequencing. *Nucleic Acids Res.* 2016;44(16):e131.

36. Mazor T, Pankov A, Johnson BE, et al. DNA methylation and somatic mutations converge on the cell cycle and define similar evolutionary histories in brain tumors. *Cancer Cell*. 2015;28(3):307–317.
37. Liao Y, Smyth GK, Shi W. FeatureCounts: an efficient general purpose program for assigning sequence reads to genomic features. *Bioinformatics*. 2014;30(7):923–930.
38. Li H. Minimap2: pairwise alignment for nucleotide sequences. *Bioinformatics*. 2018;34(18):3094–3100.
39. Li H, Handsaker B, Wysoker A, et al; 1000 Genome Project Data Processing Subgroup. The sequence alignment/Map format and SAMtools. *Bioinformatics*. 2009;25(16):2078–2079.
40. Sottoriva A, Spiteri I, Piccirillo SG, et al. Intratumor heterogeneity in human glioblastoma reflects cancer evolutionary dynamics. *Proc Natl Acad Sci U S A*. 2013;110(10):4009–4014.
41. Capper D, Reuss D, Schittenhelm J, et al. Mutation-specific IDH1 antibody differentiates oligodendrogliomas and oligoastrocytomas from other brain tumors with oligodendroglioma-like morphology. *Acta Neuropathol*. 2011;121(2):241–252.
42. Capper D, Weissert S, Balss J, et al. Characterization of R132H mutation-specific IDH1 antibody binding in brain tumors. *Brain Pathol*. 2010;20(1):245–254.
43. Kato Y, Jin G, Kuan CT, et al. A monoclonal antibody IMab-1 specifically recognizes IDH1R132H, the most common glioma-derived mutation. *Biochem Biophys Res Commun*. 2009;390(3):547–551.
44. Wang F, Flanagan J, Su N, et al. RNAscope: a novel in situ RNA analysis platform for formalin-fixed, paraffin-embedded tissues. *J Mol Diagn*. 2012;14(1):22–29.
45. Rowland TJ, Dumbović G, Hass EP, Rinn JL, Cech TR. Single-cell imaging reveals unexpected heterogeneity of telomerase reverse transcriptase expression across human cancer cell lines. *Proc Natl Acad Sci U S A*. 2019;116(37):18488–18497.
46. Schulze Heuling E, Knab F, Radke J, et al. Prognostic relevance of tumor purity and interaction with MGMT methylation in glioblastoma. *Mol Cancer Res*. 2017;15(5):532–540.
47. Aran D, Sirota M, Butte AJ. Systematic pan-cancer analysis of tumour purity. *Nat Commun*. 2015;6:8971.
48. Haider S, Tyekucheva S, Prandi D, et al; Cancer Genome Atlas Research Network. systematic assessment of tumor purity and its clinical implications. *JCO Precis Oncol*. 2020;4:PO.20.00016.
49. Gao J, Pickett HA. Targeting telomeres: advances in telomere maintenance mechanism-specific cancer therapies. *Nat Rev Cancer*. 2022;22(9):515–532.
50. Aquilanti E, Kageler L, Watson J, et al. Telomerase inhibition is an effective therapeutic strategy in TERT promoter-mutant glioblastoma models with low tumor volume. *Neuro Oncol*. 2023;25(7):1275–1285.
51. Aquilanti E, Kageler L, Wen PY, Meyerson M. Telomerase as a therapeutic target in glioblastoma. *Neuro Oncol*. 2021;23(12):2004–2013.
52. Mender I, Zhang A, Ren Z, et al. Telomere stress potentiates STING-dependent anti-tumor immunity. *Cancer Cell*. 2020;38(3):400–411.e6.
53. Yu S, Wei S, Savani M, et al. A modified Nucleoside 6-thio-2′-deoxyguanosine exhibits antitumor activity in gliomas. *Clin Cancer Res*. 2021;27(24):6800–6814.
54. Li X, Qian X, Wang B, et al. Programmable base editing of mutated TERT promoter inhibits brain tumour growth. *Nat Cell Biol*. 2020;22(3):282–288.